



Food and Liquid Sensing in Practical Environments using RFIDs

Unsoo Ha, Junshan Leng, and Alaa Khaddaj, and Fadel Adib,
Massachusetts Institute of Technology

<https://www.usenix.org/conference/nsdi20/presentation/ha>

This paper is included in the Proceedings of the
17th USENIX Symposium on Networked Systems Design
and Implementation (NSDI '20)
February 25-27, 2020 • Santa Clara, CA, USA

978-1-939133-13-7

Open access to the Proceedings of the
17th USENIX Symposium on Networked
Systems Design and Implementation
(NSDI '20) is sponsored by

 NetApp®

Food and Liquid Sensing in Practical Environments using RFIDs

Unsoo Ha, Junshan Leng, Alaa Khaddaj, Fadel Adib

Massachusetts Institute of Technology

Abstract – We present the design and implementation of RF-EATS, a system that can sense food and liquids in closed containers without opening them or requiring any contact with their contents. RF-EATS uses passive backscatter tags (e.g., RFIDs) placed on a container, and leverages near-field coupling between a tag’s antenna and the container contents to sense them noninvasively.

In contrast to prior proposals that are invasive or require strict measurement conditions, RF-EATS is non-invasive and does not require any calibration; it can robustly identify contents in practical indoor environments and *generalize to unseen environments*. These capabilities are made possible by a learning framework that adapts recent advances in variational inference to the RF sensing problem. The framework introduces an RF kernel and incorporates a transfer model that together allow it to generalize to new contents in a sample-efficient manner, enabling users to extend it to new inference tasks using a small number of measurements.

We built a prototype of RF-EATS and tested it in seven different applications including identifying fake medicine, adulterated baby formula, and counterfeit beauty products. Our results demonstrate that RF-EATS can achieve over 90% classification accuracy in scenarios where state-of-the-art RFID sensing systems cannot perform better than a random guess.

1 Introduction

The networking community has recently witnessed a surge in research that uses wireless signals for sensing liquid and food properties [25, 21, 66, 77]. This research is motivated by a desire to develop low-cost, ubiquitous solutions for food safety sensing by leveraging pervasive networking technologies. In contrast to traditional food sensing solutions which rely on expensive equipment in specialized labs, these new proposals aim to make food safety sensing accessible to lay consumers. This can help avoid widespread future health hazards like the Chinese baby milk scandal [43], the Flint water crisis [70], and the recurring alcohol poisoning problem which results in hundreds of cases of blindness and death every year [32].

Despite initial steps made toward this vision [21, 77, 66], existing proposals still have fundamental limita-

tions that make them too invasive and/or impractical for lay consumers. Specifically, they either require users to extract liquid samples and place them in specialized containers (which often involves a complex calibration process) [21, 77, 56], or they can only operate correctly a single lab setup under strict measurement conditions [66, 25]. These limitations make it difficult for consumers to use such systems for testing products for contamination or counterfeiting before purchasing and outside pre-calibrated lab environments.

The goal of this paper is to develop a *noninvasive, zero-calibration* system for wireless sensing of food and liquids in practical environments. Such a system would enable consumers to test food and liquids without opening their containers and in different environments: supermarkets, grocery stores, or homes. Our system will rely on off-the-shelf RFIDs (Radio Frequency IDentifiers), similar to those used in some past proposals [25, 66]. RFIDs cost few cents each, and they have been widely adopted by the industry as barcode replacements for billions of items (including food products). This makes them ideal candidates for low-cost and ubiquitous food sensing. Moreover, our recent research has demonstrated that an RFID’s signal changes when it is placed on containers filled with different liquids due to near-field coupling between the RFID’s antenna and material inside the container [25]. However, similar to earlier wireless proposals, this RFID-based approach could not generalize to new environments.

The difficulty in extending wireless food sensing to different environments is that radio signals are not only impacted by the content of a container but also by the environment where the measurement is made. Fig. 1 illustrates this challenge by showing three experimental trials in two different setups. Each setup consists of a wireless reader that measures the RFID’s signal and extracts the channel response. This response is impacted by two factors: the content inside the container (due to the near-field coupling) and the measurement environment which encompasses the location of the container with respect to the reader as well as the reflections off different objects in the environment (due to the propagation of the RFID’s wireless signal before it reaches the reader). As a result, if either the environment or the content proper-

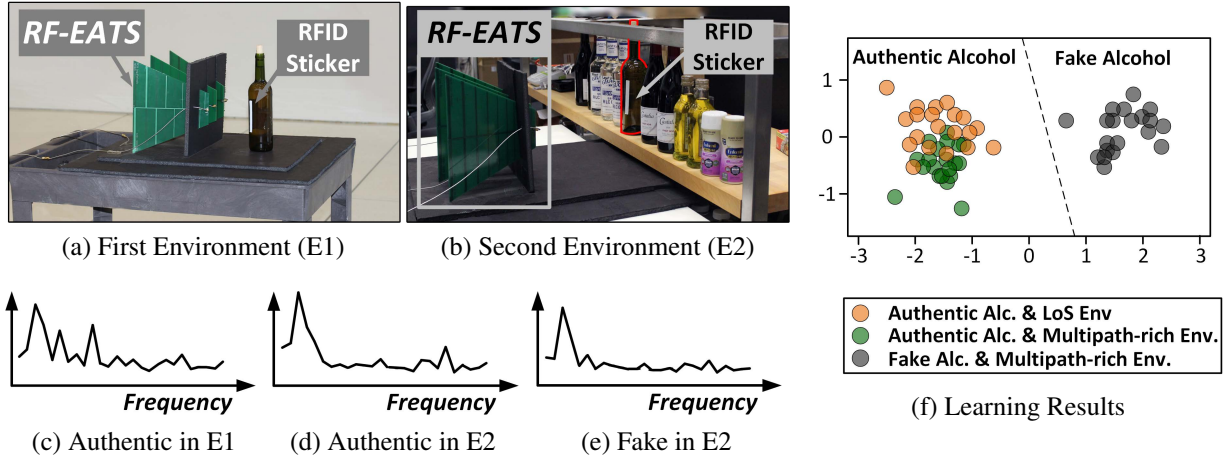


Figure 1: **RF-EATS** senses food and liquids noninvasively across different environments. The figure shows how RF-EATS uses unmodified RFID stickers placed on authentic and fake alcohol-filled bottles to sense their contents noninvasively in two different environments shown in (a) and (b). (c)-(e) plot the RFID’s wideband response from three experimental trials. Because the environment significantly impacts the measured RFID response, the frequency spectra of (d) and (e) look closer than (c) despite that (c) and (d) are from authentic alcohol bottles while (e) is from a fake alcohol one. (f) plots the classification output of RF-EATS’s learning model (after dimensionality reduction), where each point represents a different experimental trial. The plot shows that trials with authentic alcohol collected across different environments are clustered together, while those with fake alcohol are in a different cluster. This shows that RF-EATS can correctly classify contents despite the environmental changes.

ties change, the response changes (see the bottom row of Fig. 1). This is why prior proposals require calibrating or constraining the measurement conditions, limiting the practicality and generalizability of their designs.

We present RF-EATS,¹ an RFID-based sensing system that is robust to environmental variations and that generalizes well to unseen environments. At the core of RF-EATS’s design is a neural learning model that can learn RF features due to a container’s content and discard those resulting from extraneous environmental changes. For example, if the system is trained to detect adulterated baby formula in a lab environment, it still has high detection accuracy in a supermarket-style setup with dense environmental multipath (reflections) from metal shelving and other items on the aisles.

A fundamental challenge in training any neural learning model (including for image or text classification tasks) arises from the need for very large datasets. This challenge is exacerbated in our context due to the limited availability of RF datasets for sensing. A naive solution is to collect an extensive dataset that covers various indoor environments and use it in training. However, such an approach is time-consuming, inefficient, and incapable of generalizing to unseen environments.

To efficiently generalize to different environments, RF-EATS builds on recent advances in variational autoencoders [53, 33] and adapts them to RF sensing tasks. These models are typically used to generate realistic synthetic data (e.g., images of faces of humans who do not exist). Instead, RF-EATS employs them to generate a large number of realistic multipath-affected data

from a small number of real-world measurements. To do so, it introduces a *multipath kernel function*, which allows it to (approximately) decompose the wireless channel into content-dependent and environment-dependent features. Subsequently, RF-EATS can train an autoencoder to learn distributions of practical radio environments (i.e., reflections, position changes, etc.) by focusing on the environment-dependent features. This allows RF-EATS to emulate a large number of realistic measurements and use them to train its neural classifier.² In §3.1, we describe this technique in detail and demonstrate how its stochastic nature enables generalizing RF-EATS to unseen environments.

It is desirable to extend RF-EATS’s learning framework to new contents in a sample-efficient manner. For example, if a model is trained to detect adulterated baby formula, we would like to extend it to detect fake alcohol using a small number of alcohol measurements. Said differently, we would like to harness the power of a well-trained model on a large number of measurements to achieve high accuracy on new tasks, without having to train a new model from scratch. To do so, RF-EATS employs transfer learning: it divides a multi-layered network into *common layers* (shared by all tasks) and *task-specific layers*. In order to learn a new task (e.g., detecting fake alcohol), it can inherit the common layers from a well-trained model (e.g., the baby formula model) and only needs to retrain the task-specific layers. This further reduces the number samples required to extend the model to new contents, allowing RF-EATS to achieve near-

¹RF-EATS stands for RF-based Environment-Agnostic Transferable Sensing.

²In our evaluation, we demonstrate how this approach significantly outperforms using the standard ray-tracing model for generating synthetic multi-path environments [63].

optimal accuracy even when the dataset from a new content is limited. We describe this model in details in §3.2.1 and show how the common layers can serve as a pre-trained model for future classification tasks beyond those described in this paper.

We implemented a prototype of RF-EATS on USRP X310 software radios, and tested it with off-the-shelf UHF (Ultra-High Frequency) RFIDs. We adapted a recent wideband measurement technique which can extract more than half a GHz of RF measurements from off-the-shelf, passive RFIDs [40], thus providing a rich set of features for classification. We evaluated it in seven different applications and with sixteen different contents including: fake medicine, adulterated baby formula, contaminated alcohol, counterfeit perfume, wine aging, and soda classification. In each of these applications, we evaluated its ability to identify adulteration under standard contamination/adulteration levels reported in recent cases [43, 32, 50, 17, 19].

Our results from 2048 experimental trials in 20 different environments demonstrate the following:

- RF-EATS’s accuracy approaches 90% across most the above applications even when tested in new and unseen environments. In contrast, the accuracy of a state-of-the-art baseline [25] drops from 90%+ when evaluated in the same environment to a random guess in unseen environments for half the applications.
- RF-EATS’s transfer model enables achieving near-optimal accuracy with as little as four data samples, demonstrating the importance of this model when the dataset is limited.
- We show how RF-EATS’s autoencoder can be used as an anomaly detector to generalize to contaminated or counterfeit content even if it has not been trained on the specific contaminant.
- RF-EATS’s accuracy is directly impacted by the dielectric differences between the contents it wishes to classify. We show some negative results including its low accuracy in detecting fake extra-virgin olive oil due to limited dielectric differences between fake and authentic olive oil.

Contributions: RF-EATS is the first RFID-based system that can noninvasively sense food and liquids in closed containers and operate correctly in unseen environments. It employs a variational autoencoder architecture that can learn and generate realistic multipath environments, and introduces a new kernel function that can apply these generated environments to real data. It also employs transfer learning to efficiently extend its sensing capabilities to new liquids and food items. The paper also contributes a prototype implementation and evaluation of RF-EATS in practical environments.

It is important to note that RF-EATS’s performance is directly impacted by the extent of dielectric differences

between contents it wishes to classify. This means that if the dielectric differences are small (e.g., the olive oil application), the accuracy degrades. This degradation is likely to be mitigated as the dataset and learning models evolve. We also note that our evaluation focused on demonstrating robustness to changes in the surrounding environment while fixing the container’s material (e.g., glass or plastic) and shape. Despite these limitations, RF-EATS marks an important step toward food and liquid sensing in practical environments. More generally, we hope that RF-based liquid and food sensing will follow a similar trend in accuracy improvements as that witnessed by vision and text learning tasks in recent years.

2 Background

Researchers have long recognized the need for monitoring food quality and safety. Most existing techniques rely on measuring electrochemical and electrophysical properties [42, 35, 65, 1]. The process involves extracting food samples and placing them in direct contact with chemical reagents and/or specialized sensing circuits (e.g. biotoxin sensors [15, 16, 27]) and is typically done in specialized food labs.

Given the length of the food lab testing process, recent proposals have considered building small sensing circuits in hope of incorporating them inside food containers [72, 46, 62, 51, 37]. These proposals require designing a customized sensor for every different type of food or food property of interest [72, 62] or they require coating existing circuits (e.g., LC circuits or RFIDs) with different types of polymers to increase sensitivity to specific materials of interest [46, 51]. Moreover, many of these sensors still require direct contact with food samples, which can lead to contaminating the food samples and is erosive to their sensing interfaces [47, 76, 58].

The desire for ubiquitous and general purpose solutions has led networking and mobile researchers to explore various mobile sensing modalities. These techniques rely on different kinds of wireless signals to extract material properties such as the electric permittivity [66, 21, 23, 44, 78], surface tension [60, 71, 77], or photo-acoustic signatures [57]. However, the reliance on wireless signals makes these techniques highly sensitive to measurement conditions; hence, the proposed systems require isolating food samples of interest and placing them in calibrated setups. This includes recent proposals like LiquID [21], TagScan [66], and CapCam [77]. The invasiveness of these approaches makes them unsuitable for use by consumers before they purchase counterfeit or contaminated food and liquid products. RF-EATS shares the vision of this line of work but aims to develop a non-invasive approach for food and liquid sensing.

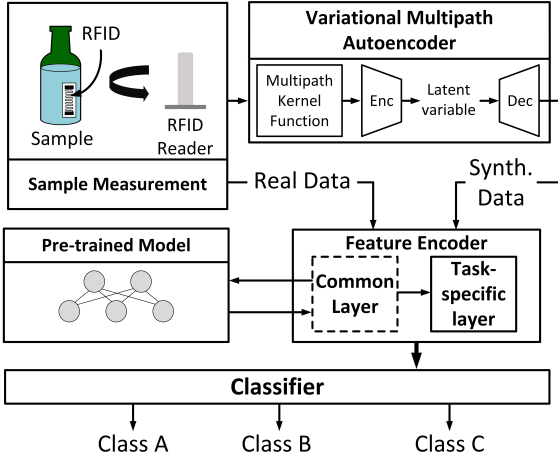


Figure 2: RF-EATS’s Learning Model.

3 Design

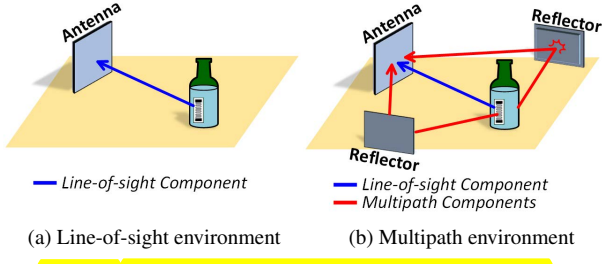
RF-EATS is a wireless system that can noninvasively sense food and liquid products in closed containers without opening them. It relies on cheap, passive UHF (Ultra-High Frequency) RFID tags placed on the containers, and exploits the near-field coupling between the RFID’s antenna and the container’s contents. These RFIDs may either be already affixed on the container by the manufacturer, or they may be attached as stickers to the container as shown in Fig. 1.

Fig. 2 shows the overall system architecture. From the hardware perspective (top left), it uses a modified RFID reader capable of obtaining wideband channel measurements [39, 25, 14] of unmodified RFID tags. The reader sends a downlink signal which powers up a passive tag and obtains the tag’s response. It performs standard channel estimation using the packet preamble, and uses the channel estimates in training and classification.³ Note that while our discussion focuses on a single tag, it can be easily extended to any number of tags since it adapts the standard EPC-Gen2 protocol.

RF-EATS can be used for various inference tasks (e.g., detecting adulterated baby formula, fake alcohol). Its learning architecture consists of a neural network with the following components, as shown in Fig. 2:

- *Variational Multipath Autoencoder* (§3.1): This component takes as input a small number real-world channel measurements and outputs a large number of realistic synthetic measurements. At the heart of this component is a multipath kernel function that enables learning representative distributions of RF environments while discarding the container contents’ impact.
- *Feature Encoder* (§3.2.1): This component takes as input real and synthetic data and extracts features for use in classification. It consists of multiple layers, some of

³It relies on the channels not the IDs for the inference tasks.



(a) Line-of-sight environment (b) Multipath environment

Figure 3: Typical Ray-Tracing Channel Approximations.

which are shared among all classification tasks. These layers may be reused as a pre-trained model for extending RF-EATS to new types of contents.

- *Classifier* (§4.1): The component takes as input the features outputted by the feature encoder, and outputs the classification results. While the variational autoencoder and part of the feature encoder are shared by all tasks, this component must be retrained for each task.

The above three components together enable RF-EATS to generalize to unseen environments (through synthetic data from the autoencoder), expand to new materials using small datasets (by leveraging the shared layers of the feature encoder), and extend to untested contaminants (by using the autoencoder as an anomaly detector). The following sections explain these components in details.

3.1 Variational Multipath Autoencoder

To achieve high accuracy with a neural learning model, RF-EATS’s training dataset needs to be large and representative of a variety of environments. Unfortunately, collecting large datasets for every contaminant and every multipath environment is an expensive and time-consuming [28]. Further, even if we manage to collect such datasets, there would remain unseen environments which the model may not be able to generalize to.

Below, we describe how RF-EATS overcomes this challenge by leveraging a stochastic generative model based on variational autoencoders. The model enables it to generate realistic synthetic data for use in training, which increases its accuracy despite limited datasets and enables it to generalize to unseen environments.

3.1.1 The Multipath Kernel

RF-EATS’s generative model needs to realistically capture different aspects of an RFID’s measured channel response. Fig. 3(a)-(b) depict common approximations of the wireless channel. In line-of-sight scenarios, the RFID’s wireless signal arrives on a direct path to the reader’s antenna; in multipath-rich environments, the signal arrives on multiple paths (after bouncing off various reflectors) which linearly combine at the receiver. Mathematically, the RFID’s channel h at a given frequency k is typically approximated as [63]:

$$h_k = \sum_{i=0}^N a_i e^{-j2\pi f_k \tau_i} \quad (1)$$

where a_i and τ_i are the amplitude and time delay of the i^{th} path, f_k is the k^{th} frequency, and N is the total number of paths.

This standard approximation is problematic for RF-EATS's learning tasks because of two main reasons: 1) it ignores the impact of the RFID's antenna gain and 2) it ignores scattering and diffraction phenomena of radio signals. The first approximation is particularly detrimental since it prevents capturing the impact of the container's content on the antenna (more specifically, the impact of the content's dielectric ϵ). The second one is also problematic as it results in less representative channel distributions.⁴ While it is possible to overcome these shortcomings by solving Maxwell's equations [64], this is undesirable since it requires precise modeling of the geometry and materials in the environment, making it practically and computationally expensive [61].

To truthfully represent the RFID's measured response, we would like RF-EATS's generative model to embrace the complexity of the wireless channel. The model must incorporate both the impact of the content dielectric (on the antenna gain) and that of the wireless signal propagation (due to reflection, scattering, and diffraction). We can achieve this by expressing the overall channel as a product of the gain $G(\epsilon, k)$ and the propagation $P(k)$ characteristics as follows:

$$h_k = G(\epsilon, k) \cdot P(k) \quad (2)$$

We make the following remarks:

- First, one might wonder why the presence of other nearby objects does not impact the RFID's antenna gain (i.e., why it only affects the propagation factor $P(k)$). To answer this question, we note that the electromagnetic interaction of antennas with different objects in the environment depends on the distance between the antenna and the objects [29]. If an object is in the near-field (i.e., within one wavelength⁵), it "couples" with the antenna and impacts its gain. If the object is in the far-field (i.e., larger than two wavelengths), it impacts the propagation $P(k)$. This is why RF-EATS incorporates the impact of container contents into the gain while absorbing environmental multipath into the propagation factor.⁶
- If the location and multipath environment are fixed, then any change in the measured channel h_k can be attributed to the gain $G(\epsilon, k)$ and thus be used directly

⁴In §4.4, we empirically compare against the standard ray-tracing model and show that RF-EATS significantly outperforms it.

⁵In the UHF ISM band, the wavelength is about 30 cm. It becomes significantly smaller in liquids due to the impact of the dielectric.

⁶This approximation works well in practical because near-field backscatter power decays as $1/d^4$.

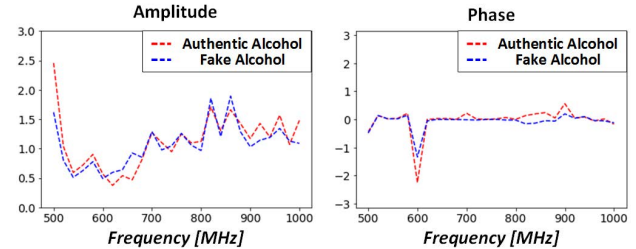


Figure 4: Output of Multipath Kernel Function.

to infer the contents. Indeed, this is why past proposals for wireless food sensing required fixing and/or calibrating their setup but are unable to generalize to different multipath environments.

- Similarly, if the content of a container is fixed, then any change in the measured channel can be attributed entirely to the multipath environment $P(k)$. Let us say that we measure the RFID's channel in two scenarios: one in a line-of-sight (LOS) controlled environment with little to no multipath ($h_{k,LOS}$), and another in a multipath-rich environment ($h_{k,M PATH}$). The ratio of these measurements is entirely dependent on the multipath environment and independent of a container's contents. Specifically:

$$\frac{h_{k,M PATH}}{h_{k,LOS}} = \frac{P_{M PATH}(k)}{P_{LOS}(k)}$$

We call this the *multipath kernel function*. For simplicity, we approximate a multipath-free $P_{LOS}(k) \approx 1$.

To test that the multipath kernel indeed results in content-independent features, we ran experimental trials with fake and authentic alcohol in two environments representing line-of-sight and multipath-rich settings similar to those shown in Fig. 1. We computed the ratio of the channel in multipath to that in line of sight, and plot the output in Fig. 4. Since the channel is a complex number, we plot the amplitude and phase of the ratios on separate graphs, each as a function of frequency. The figure shows that the ratio is indeed independent of the content since the plots for authentic (red) and fake (blue) alcohol almost overlap for both magnitude and phase. This indicates that the kernel function enables us to extract environment-dependent content-independent features.

3.1.2 Training a Generative Model

Now that we have a mechanism to obtain environment-dependent features from real-world measurements, we can use them to train a generative model. The model takes these measurements as input and generates a large number of synthetic data representing different multipath environments. While there are various kinds of generative models [55, 53, 33], RF-EATS employs variational autoencoders (VAE) because they have the ability to generalize using a small input dataset. In what follows, we

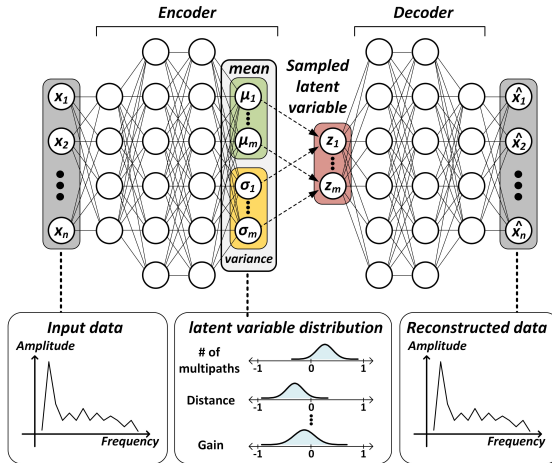


Figure 5: RF-EATS’s Variational Autoencoder.

describe these models at a high level and in the context of our problem, and we refer the interested reader to [53] for a more detailed exposition.

VAEs assume that the input features represent a much lower dimensional space of latent variables. In the context of our learning tasks, the wireless propagation factor is indeed caused by a small number of reflectors and scatterers in the environment [34]. However, the reflectors and scatterers change across different environments, resulting in different channel responses. VAEs capture this phenomenon by assuming that the latent variables are randomly drawn from a normal distribution. Once the underlying distributions are learned, RF-EATS can draw new samples from them to generate synthetic data for unseen multipath environments.

Fig. 5 shows the overall architecture of RF-EATS’s variational autoencoder. The VAE takes as input the channel ratios, each of which consists of a multi-dimensional vector x_1, x_2, \dots, x_n , and outputs a reconstruction of these features $\hat{x}_1, \hat{x}_2, \dots, \hat{x}_n$. The model consists of an encoder (which aims to compress these features into latent variables z_1, z_2, \dots, z_m) and a decoder (which aims to reconstruct the input from the latent variables). By compressing and decompressing the input, the neural network aims to learn a representative lower-dimensional distribution of the latent variables.

Formally, the purpose of training the VAE is to learn the parameters of the neural network that can (1) minimize the reconstruction loss between the input x and output \hat{x} , and (2) model the underlying distribution of the latent variables $q_\theta(z|x)$ as a normal distribution. Formally, this can be achieved by minimizing the following loss function [33]:

$$L_i(\phi, \theta, x_i) = KL(q_\theta(z|x_i)||\mathcal{N}(0, 1)) + \mathcal{L}(x, \hat{x}) \quad (3)$$

where KL is Kullback-Leibler divergence, which is a measure of the difference between two probability distributions, $\mathcal{N}(0, 1)$ denotes the Gaussian with zero mean and standard deviation of 1, and \mathcal{L} represents the L_2 norm of the reconstruction loss in frequency domain.

The following points are worth noting:

- The VAE input and output are independent of the content. Hence, it can be trained on any container content (or even on empty containers), and its output may be used for any classification task as we explain below.
- Our discussion focuses entirely on the RFID’s channel and ignores the communication bits. This is possible because RF-EATS applies standard channel estimation on the RFID packet’s preamble to extract the channel. It also uses an out-of-band sensing technique (described in §4.1) to obtain wideband estimates.

3.1.3 Embedding Dielectric Characteristics

Once the VAE has been trained, it can be used to generate synthetic multipath environments by randomly drawing samples z from the latent distributions and passing them through the decoder shown in Fig. 5. Note, however, that the VAE’s synthetic output cannot be directly used to train a contamination classifier (i.e., we cannot directly use it to train a fake alcohol classifier). This is because output features are independent of the content.

In order to generate synthetic measurements that incorporate the impact of both the content and the propagation environment, we need to apply the inverse of the multipath kernel. Specifically, we need to measure $h_{k,LOS}$ of an RFID placed on fake and authentic alcohol bottles in line-of-sight settings, then multiply these measurements by the output features of the VAE. Since the generative model is capable of stochastically generating different multipath environments, we only need a small measurement dataset of $h_{k,LoS}$ to generate a large number of realistic channel measurements and feed them into the classifier. Hence, the VAE model provides a large corpus for training the classifier without requiring measurements for every multipath environment and contaminant.

3.2 Extending to New Tasks and Compositions

In this section, we describe how we can efficiently extend RF-EATS’s learning framework to new tasks and unseen compositions or contaminants.

3.2.1 Transfer Learning to New Tasks

We would like to extend RF-EATS to new classification tasks in a sample-efficient manner. For example, having trained a classifier to detect fake alcohol using a large dataset, we would like to extend it to detect adulterated baby formula using a small number of samples. This would enable expanding RF-EATS to new tasks using a smaller number of measurements of the new content of interest. To do so, RF-EATS employs transfer learning in order to transfer training knowledge from a well-trained source domain (e.g., alcohol) to a new target domain (e.g., baby formula).

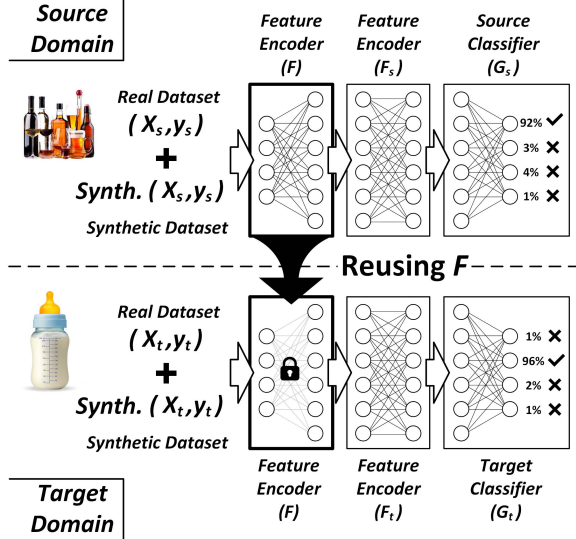


Figure 6: RF-EATS’s Transfer Learning Model.

Fig 6 shows how this process works at a high level. Recall that neural networks consist of multiple layers, some of which are used for feature extraction or encoding, while others are used for classification. The feature extraction layers themselves may be further divided into common layers and task-specific layers. The common layers can be directly transferred as “frozen” layers F from a well-trained classifier to the target domain. This significantly reduces the number of parameters that need to be learned for the new task, thus reducing the required dataset size to achieve high accuracy.

Mathematically, each domain can be represented as

$$\begin{aligned}(X_s, y_s) &= \{(x_{s,i}, y_{s,i})\}_{i=1}^{N_s} \\ (X_t, y_t) &= \{(x_{t,i}, y_{t,i})\}_{i=1}^{N_t}\end{aligned}\quad (4)$$

where X_s and y_s are the observations and respective labels of the source content domain, X_t and y_t are the observations and labels of the target content domain, x_i represents the complex channel estimate of one observation over different frequencies, y_i represents the label (e.g. contaminated or not), N_s the number of samples in the source content domain and N_t the number of samples in the target content domain.

Assuming the latent space dimensionality is d , we can represent the feature encoder and source/target classifier as:

$$F : \mathbb{R}^n \rightarrow \mathbb{R}^d$$

$$G_s \circ F_s : \mathbb{R}^d \rightarrow \{0, 1, \dots, C_s\} \quad (5)$$

$$G_t \circ F_t : \mathbb{R}^d \rightarrow \{0, 1, \dots, C_t\}$$

where n comes from the dimension of the input data, and C_s, C_t represent the number of classes in the source and target content domains respectively.

After training the model on the source content domain, we fix the weights of F . We then compute $\hat{y}_t = G_t \circ F_2 \circ F(X_t)$ and minimize the standard cross-entropy loss

Algorithm 3.1 VAE-based Anomaly Sample Detection

Input: Anomalous data point x_i , threshold α , trained Encoder E_θ and Decoder D_ϕ

Output: Reconstruction probability P_R

$$\mu_{z(i)}, \sigma_{z(i)} = E_\theta(x_i)$$

draw L samples from $z \sim N(\mu_{z(i)}, \sigma_{z(i)})$

for $l = 1$ to L do

$$\hat{x}_{(i,l)} = D_\phi(z_{(i,l)})$$

$$P_{R(i)} = \frac{1}{L} \sum_{l=1}^L \mathcal{L}(x, \hat{x}_{(i,l)})$$

if $P_{R(i)} > \alpha$ then

x_i is an anomaly

else

x_i is not an anomaly

function $\mathcal{L}_t(y_t, \hat{y}_t) = -\sum_{i=1}^C p(y_{t,i}) \log p(\hat{y}_{t,i})$, where $y_{t,i}$ and $\hat{y}_{t,i}$ represent the actual and predicted label for class i . Here, only the weights of F_2 and G_t are updated, while the weights of F remain intact.

3.2.2 Anomaly Detection for Unseen Compositions

So far, we have assumed that RF-EATS’s classifiers have been trained on samples from all classes of interest, including counterfeit and adulterated samples. However, in many practical applications, we may not have access to counterfeit or contaminated samples, or the composition/type of contaminant may be unknown.

We can generalize RF-EATS to deal with such situations by using its VAE as an anomaly detector [13, 41]. Recall that the VAE is trained to minimize the reconstruction loss of the environment-dependent features. Hence, if the input to the VAE encodes environment-dependent features, we expect the reconstruction loss to be low. On the other hand, if the input deviates from the expected distribution, the reconstruction loss will be high, indicating an anomaly.

To see how this can be used to detect counterfeiting, consider the case of a manufacturer that creates a database of $h_{k,LOS}$ measurements of the authentic product. Subsequently, if we measure the channel $h_{k,c}$ of a counterfeit product and apply the multipath kernel to it, we obtain:

$$\frac{h_{k,MPATH}}{h_{k,LOS}} = \frac{P_{MPATH}(k)}{P_{LOS}(k)} \times \frac{G(\varepsilon', k)}{G(\varepsilon, k)}$$

Notice how in such situations, the impact of the content does not cancel out upon applying the multipath kernel, and the resulting ratio is not only dependent on the environment P , but also on the content. Thus, if this ratio is fed as input to the VAE, we expect a high reconstruction loss since the sample deviates from the learned distribution. In contrast, if the sample were authentic, the ratio will be dielectric-free and the reconstruction loss would be lower. Algorithm 3.1 summarizes the anomaly detection algorithm using the variational autoencoder.

4 Implementation and Evaluation

4.1 Implementation

Hardware. We implemented our design on USRP X310 and N210 software radios [11] by extending a two-frequency excitation prototype [40]. The radios run the EPC-Gen2 protocol and transmit two frequencies: one high power frequency (10-31dBm) inside the UHF ISM band and another low power sensing frequency which is varied within 500-1000 MHz. At the sensing frequency’s receiver, we employed a low-pass filter that eliminates the impact of the power up frequency and added an LNA to boost the received signal power. To reduce the harmonics of transmission, we used a low-pass filter at the output of the transmit USRPs. We also added anti-aliasing low-pass filters at the input of the receive USRPs. The received signal is sampled (digitized) and sent over Ethernet to a computer for offline processing.

Software. RF-EATS’s software package was implemented in MATLAB and python. The transmitted query requests the extended RFID preamble, and the receiver averages 50 RFID responses to boost the signal-to-noise ratio (SNR). The receiver decodes the response and performs standard channel estimation using the packet preamble. It repeats this process over 26 frequencies, separated by 20 MHz across RF-EATS’s 500 MHz frequency span. This results in RF-EATS’s feature vectors which include amplitude, phase, and correlation across frequencies. The multipath kernel was applied by dividing the multipath-affected data by line-of-sight measurement data ($h_k/h_{k,LoS}$). The number of datapoints used in training the classifiers is much larger than the number of measurements due to this combinatorial relationship.

To ensure the reliability of the channel measurements (i.e., that the channel estimates were not significantly distorted by noise or interference), we computed the correlation at each frequency k as:

$$corr_k = \sum_t y_t p_t^* / \sqrt{\sum_t |y_t|^2 \sum_t |p_t|^2} \quad (6)$$

where p_t is the known preamble of the RFID packet and y_t is the received signal. We discarded points that had very low (≤ 0.6). We used the python implementation of the PyTorch and Keras package [49] to implement RF-EATS’s classifier and refiner.

Transfer Learning Classifier. The classifier was implemented as a fully-connected network with 3 hidden layers. Dropout and batch normalization layers were added to minimize overfitting. We used the Adam optimizer and set learning rate = $1e-4$, $beta1=0.9$, $beta2=0.999$, $dropout\ rate=0.2$.

Variational Autoencoder. The encoder and decoder were implemented as fully-connected networks with 3 hidden layers each. The dimension of latent variable was

Content	Samples	Content	Samples
Pure Alcohol	218	Baby Formula (uncontaminated)	95
Diluted Alcohol (10% water)	218	Baby Formula (Contaminated)	94
Tainted Alcohol (10% methanol)	218	Extra Virgin Olive Oil (unadulterated)	80
Coke	218	Extra Virgin Olive Oil (adulterated)	79
Pepsi	218	Wine (2009)	77
Diet Coke	116	Wine (2012)	76
Real Perfume	102	Fake Medicine	68
Counterfeit Perfume	103	Real Medicine	68

Table 1: Number of Samples per Material

set to 16. We used the Adam optimizer and set learning rate = $1e-7$, $beta1=0.9$, $beta2=0.999$, $dropout\ rate=0.2$.

4.2 Dataset & Applications

We tested RF-EATS in 7 different applications and collected 2,048 data samples in total. The applications demonstrate the generality of the technique to important real-world tasks. Below, we describe these applications, their motivations, and how their corresponding compositions were obtained. The dataset is detailed in Table 1.

- **Tainted Alcohol and Diluted Alcohol.** Tainted alcohol is an ongoing problem in many developing world countries including China, Indonesia, Iran, Turkey, India, and Mexico [32]. Alcohol is tainted by mixing it with cheaper methanol, and consuming it leads to hundreds of cases of blindness and death every year. Standard tainting percentages range between 30-50%. In order to stress-test for sensitivity, we prepared tainted alcohol by removing 10% of the content of an authentic bottle of GRAVES Grain Alcohol [8] and replacing it with methanol.
- **Adulterated Baby Formula.** In 2008, the Chinese milk scandal broke out after the hospitalization of 50,000 babies due to kidney damage [43]. Manufacturers had watered down baby formulas up to 83% and mixed them with melamine CAS NO. 108-78-1 [24], a compound used in making plastics. The purpose of adding melamine (by manufacturers) was to conceal dilution by artificially increasing protein levels. To stress-test the sensitivity of our system, we prepared adulterated baby formula by diluting a bottle of Enfamil NeuroPro Infant Formula - Ready to Use (8 fl Oz) [6] with 50% water and mixing it with a higher concentration of melamine (1g/L).
- **Fake Medicine.** Fake medicine is also a major challenge in many developing-world countries, leading to dozens of fatalities every year [50]. A recent incident involved fake cough medicine bottles, where 90% of the active ingredient was replaced with diethylene glycol, a compound used in making antifreeze agents [54]. To prepare such samples, we removed

80% of the contents of a Tylenol bottle [3] and replaced it with diethylene glycol.

- **Fake Extra-Virgin Oil.** Recent studies have shown that 69% of US-imported Extra Virgin Olive Oil has been adulterated by mixing it with cheaper oils (*e.g.*, peanut oil) [26]. This can lead to health hazards for consumers with (peanut) allergy. Standard adulteration levels range between 70-80% [26]. We prepared fake olive oil by removing 80% a bottle of GOYA Extra Virgin Olive Oil [7] and replacing it with peanut oil from Planters 100% Pure Peanut Oil.
- **Counterfeit Perfume.** Counterfeit beauty products are abound, leading Estee Lauder to confiscate over 2.6 million counterfeit items in 2016 alone [17]. Many such products are sold online. We purchased an authentic Chanel perfume (COCO MADEMOISELLE - Eau de Parfum) directly from the supplier (160\$) and a knock off for \$40 from an online retailer.
- **Wine Fraud.** Wine fraud takes many forms. A common one involves selling consumers wine vintages that are dated to earlier years, artificially inflating their price [19]. We purchased wine vintages of Castalia Pinot Noir from two different years: 2009 and 2012.
- **Soda Brand.** Counterfeit soft drinks are marketed under common brand names [4]. While it was difficult for us to purchase counterfeit soft drinks, we tested RF-EATS’s ability to classify between common brands: Coke, Pepsi, and Diet Coke.

4.3 Evaluation

Environments & Setup. We evaluated RF-EATS in 20 environments in total including supermarket-style setups with dense metal shelving, kitchens (with sinks and fridges), open lab spaces, offices, hallways and corridors, dining table settings, etc. These environments were fully furnished with tables, chairs, and computers. People walked around during our measurements, and various wireless technologies were present (LTE, WiFi, Bluetooth, etc.). Fig. 1 shows two sample setups, one representing an open lab space and another emulating a supermarket environment.⁷ In each experimental trial, a container with an RFID was placed within 10-20 cm distance and -45°-45° from RF-EATS’s antennas. The device powers up the RFID and captures its response. Across our trials, we varied the measurement conditions by changing the location of the container and the number, location, and kinds of objects/reflectors around it. Note that even though the RFID is relatively close to RF-EATS’s antennas,⁸ the richness of the multipath environment significantly impacts the measured response.

⁷Most of our trials (aside from the line-of-sight measurements) were performed outside the clean open space environments.

⁸Beyond such distance, it is difficult to power up an RFID on liquid-filled containers.

RFIDs. We performed our experiments with a variety of commercial off-the-shelf passive UHF RFIDs, including the Alien ALN-9640 Squiggle [2] and Smartrac [59] tags. Each tag costs around 5 cents.

Ground-truth. To measure the ground truth dielectric constant, we used a vector network analyzer, the Agilent Technologies E8362B PNA Network Analyzer [5] (price~\$20,000), and connected it to an N1501A dielectric probe [9]. We measured the dielectric constants across 500-1000 MHz frequency range for each content.

Baselines. Our baseline evaluation focused on non-invasive proposals (*i.e.*, we avoided past systems that are invasive or require isolating liquid samples, *e.g.*, [21, 77]). We implemented the following baselines:

- **RFIQ (Gradient Boosting)** [25]: We implemented RFIQ’s gradient boosting tree model. We set $eta = 0.3$, $max_depth = 3$, $subsample = 0.5$, and $num_boost_round = 128$.
- **VAE with a Ray-Tracing Model;** We implemented a VAE that is trained on an analytical ray-tracing model. Specifically, rather than collecting $h_{k,M PATH}/h_{k,LOS}$ in a data-driven fashion, we modeled it using the following equation:

$$\frac{h_{k,M PATH}}{h_{k,LOS}} = \sum_i a_i e^{-j2\pi f_k \tau_i} \quad (7)$$

where a_i and τ_i are the amplitude and time delay of the i^{th} path, and f_k is the k^{th} frequency. This model allows us to generate a large number of synthetic multipath environments and use them in training.

- **Simple Neural Network:** We also implemented a 3-layer fully-connected neural network, which has the same structure with RF-EATS’s neural network (but without the transfer learning and VAE components).

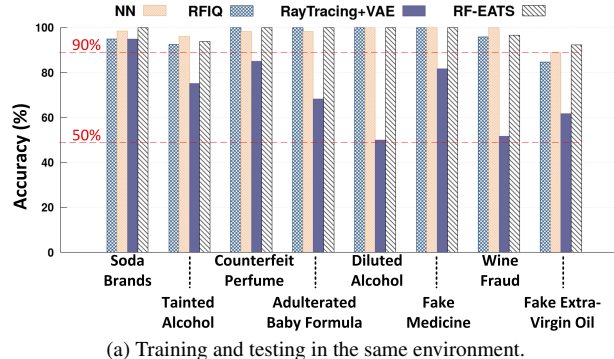
We note the following additional points:

- Across our evaluation, the dataset was divided into a training, testing, and validation sets, all mutually exclusive, *i.e.*, none of the containers or measurements used in one of these sets was present in any other sets.
- We trained the VAE using measurements taken from an RFID placed on empty containers. Recall that the VAE is content-agnostic and general.
- Similar to standard machine learning approaches, we extensively explored the space of hyper-parameters and scaling functions in our training process.

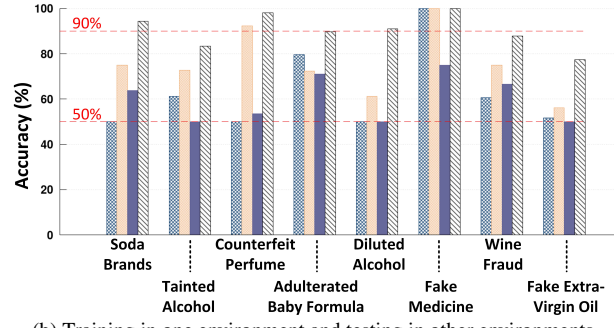
4.4 Results

4.4.1 Overall Performance

We would like to evaluate RF-EATS’s overall performance in two different regimes: the first involves training and testing in the same environment, while the second involves training in one environment and evaluating in all



(a) Training and testing in the same environment.



(b) Training in one environment and testing in other environments.

Figure 7: **Overall Performance** (a) and (b) plot the accuracy for each of the applications with different experimental regimes.

other environments. In the first regime, the dataset from all environments was mixed and divided into mutually-exclusive training and testing sets. The split-ratio is 80% training and 20% testing for both RF-EATS and the state-of-the-art baseline, RFIQ.⁹

Fig. 7 plots the accuracy for each of the applications in both regimes, and compares them to each of the baselines described in §4.3. We make the following remarks:

- When trained and tested in the same environment, most models achieve high accuracy ($\geq 90\%$) across all applications. In such scenarios, RF-EATS matches or exceeds the performance of the baselines.
- When testing in new and unseen environments, the accuracy of all the baselines drop significantly, some to a random guess. On the other hand, RF-EATS’s accuracy remains around or above 90% for six out of the eight applications, and above 83% for all the applications. Its median improvement over a simple neural network is 15.1%, over RFIQ is 26.5%, and over the ray-tracing model is 29.0% across these applications. This shows that RF-EATS’s model can indeed learn representative multipath distributions and generalize to unseen environments.
- The neural network (VAE) trained with a ray-tracing model achieves the worst performance. As discussed in §3.1.1, this is because the ray-tracing model ignores

⁹Note that we experimented with different splitting ratios and found that RF-EATS outperformed RFIQ irrespective of the split ratio.

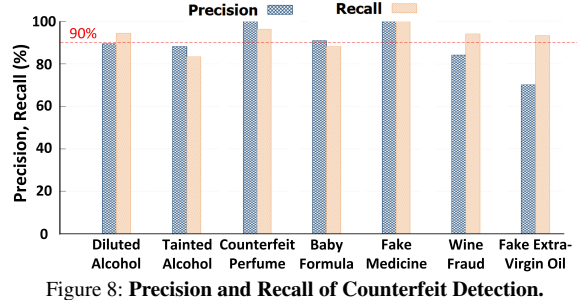


Figure 8: **Precision and Recall of Counterfeit Detection.**

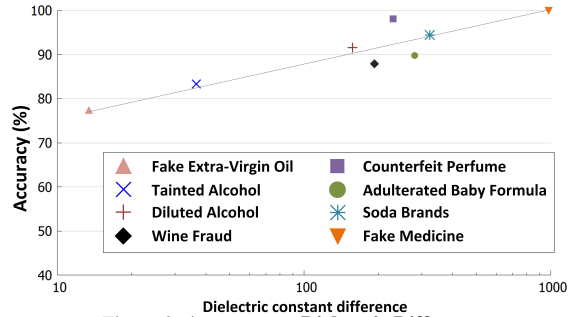


Figure 9: **Accuracy vs Dielectric Differences.**

important radio propagation characteristics. As a result, a VAE trained on such a model cannot capture representative distributions and is significantly outperformed by RF-EATS’s approach which leverages the multipath kernel.

Next, we would like to gain more insight into RF-EATS’s performance as a counterfeit detector. In counterfeit detection, it is important to understand the impact of false positives and false negatives. The standard metrics for quantifying them are denoted by precision and recall [10]:

$$Precision = \frac{TP}{TP + FP}, \quad Recall = \frac{TP}{TP + FN} \quad (8)$$

where TP is true positive, FP is false positive, and FN is false negative. Fig. 8 shows the precision and recall, demonstrating that they are of the same order of RF-EATS’s overall accuracy.¹⁰ Note that these metrics are not reported for soda brand application since false positives/negatives are not meaningful in that context.

Impact of Dielectric Difference on Accuracy. Next, we would like to confirm that RF-EATS’s performance depends on the dielectric differences between the contents of interest. We measured the dielectric of the various contents using the ground truth probe described in §4.3.¹¹ Because the dielectric constant changes with frequency, we computed the following dielectric distance metric $\sum_{i=1}^L \mathcal{L}(D_{A,i}, D_{B,i})$ where \mathcal{L} is $L2norm^{12}$ and

¹⁰The accuracy plotted in Fig. 7 can be expressed as: $(TP+TN)/(TP+TN+FP+FN)$.

¹¹Our measurements are provided in Appendix A.

¹²Note that it is possible to use other distance metrics.

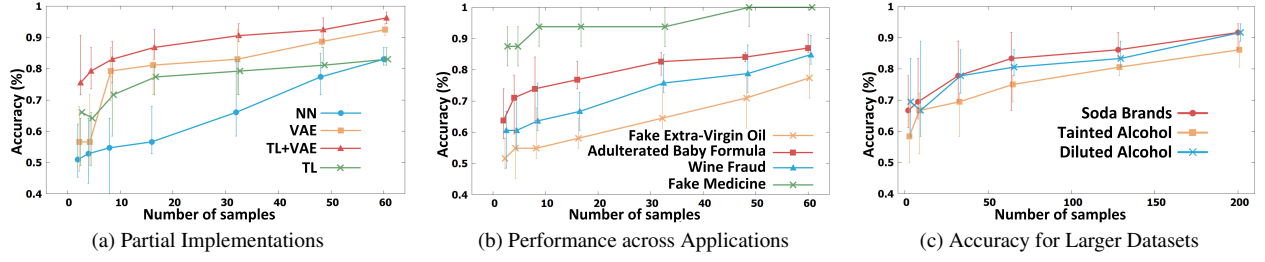


Figure 10: **Micro-benchmarks** The figure plots the median accuracy as a function of the training dataset for (a) partial implementations, (b) different applications, and (c) large dataset sizes. Error bars indicate lowest and highest accuracy for different dataset splits between training and testing.

$D_{A,i}, D_{B,i}$ are the dielectric constants at i -th frequency component of samples A and B.

Fig. 9 plots the classification accuracy as a function of the dielectric difference for each of the tasks. The figure shows a log-linear relationship between the accuracy and the dielectric differences. When the difference is over 200, RF-EATS achieves 90+% accuracy. The figure also shows that the olive oil application has the lowest accuracy and lowest difference of 15. These results verify that RF-EATS’s performance is directly impacted by extent of dielectric differences between the contents of interest.

4.4.2 Micro-benchmarks

We would like to quantify the accuracy gains arising from each of RF-EATS’s subcomponents. To do so, we evaluated the accuracy of partial implementations of the overall system: (1) a simple neural network,¹³ (2) with the VAE (but no transfer learning), (3) with transfer learning (but no VAE), (4) RF-EATS’s full architecture with both the VAE and transfer learning. Similar to our earlier evaluation, we trained on one environment and evaluated on the rest. Additionally, when training the transfer learning model on a given task (e.g., counterfeit perfume), the source domain is obtained by training the encoder on datasets from all the other tasks.

Fig. 10(a) plots the accuracy as a function of the size of the training dataset for each of the above models. For simplicity, the figure only plots results for the counterfeit perfume application. For each dataset size, we randomly chose samples from the database for training, while the rest were used for testing. We repeated this experiment ten times, each time randomly choosing a different subset of samples. The figure plots the median accuracy, and the error bars indicate the maximum and minimum accuracies across the ten iterations.

We make the following remarks:

- Each of the subcomponents contributes to the overall system performance. The improvement in accuracy from the transfer learning classifier over a simple neural network shows that the transfer classifier has higher start point, and VAE has higher slope and

¹³We also experimented with networks consisting of more than three layers, but they performed worse. This is likely due to overfitting to the small datasets, so we do not report their results.

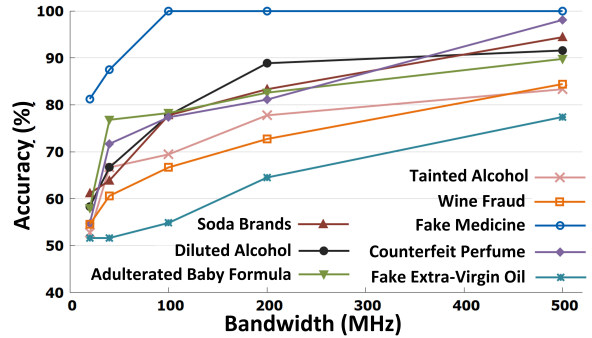


Figure 11: **Impact of Bandwidth on Accuracy.**

asymptote. This is because when the dataset is very small, transfer learning allows extracting well-defined general features and can contribute more to the overall accuracy. However, when the data size becomes large enough, the VAE has higher accuracy because of its effectiveness in generalizing to unseen environments.

- The accuracy gains are more pronounced for smaller datasets. Moreover, the overall system has a smaller standard deviation in comparison to the simple baseline. This result demonstrates the model’s ability to not just improve accuracy but also reduce the dataset size required for training.
- The accuracy of each of the models increases with the dataset size. This holds true not only for the perfume classifier but for all classification tasks as shown in Fig. 10(b)-(c), and it is expected because more data enables the learning model to better train its classifier.

Next, we would like to understand the impact of the estimation bandwidth on RF-EATS’s accuracy. Recall that our implementation uses two-frequency excitation to sense an RFID’s response over a wide bandwidth. To evaluate the impact of bandwidth on accuracy, we used the same measurements from the experimental trials performed earlier, but we only provided varying chunks of bandwidths in training and testing the learning model.

Fig. 11 plots the accuracy on the y-axis as a function of the bandwidth for each of the classification tasks. It shows that RF-EATS’s accuracy increases with bandwidth for all of the tasks. In contrast, when using a bandwidth that is constrained to the UHF ISM band (26MHz) as with a standard RFID reader, the accuracies across

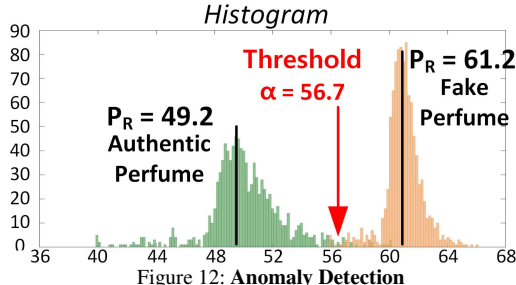


Figure 12: Anomaly Detection

most tasks are close to a random guess. This demonstrates the importance of wideband estimation for enabling RF-based food and liquid sensing.

4.4.3 Extending to Unseen Compositions

Finally, we would like to evaluate RF-EATS’s ability to perform anomaly detection as per §3.2.2. To do so, we trained the VAE on outputs of the multipath kernel obtained from all datasets except the perfume dataset. Then, we applied the multipath kernel to both the counterfeit and non-counterfeit perfume. Specifically, we compute $h_{k,MPATH}^a/h_{k,LoS}^a$ and $h_{k,MPATH}^a/h_{k,LoS}^a$ where $h_{k,MPATH}^{a/f}$ denotes the channel of authentic/fake perfume in multipath-rich environments, and $h_{k,LoS}^a$ denotes the line-of-sight channel of authentic perfume. The detector is provided with samples of $h_{k,LoS}^a$ knowing that they are authentic. We set $L = 1000$ in Algorithm 3.1, resulting in 1,000 reconstruction loss values.

Fig. 12 shows the histogram of the reconstruction loss of authentic (green) and fake (orange) perfumes. The figure shows that the average reconstruction loss of fake (61.2) is significantly smaller than that of the authentic (49.2) perfume. If we set the threshold value α to 56.7, we would obtain 94% accuracy in counterfeit detection.

5 Other Related Work

(a) RF sensing. RF-EATS is related to a large and emerging body of literature on using wireless signals for sensing purposes, including shape-based object classification [75, 74], radio localization [73, 31], liquid level sensing [18], and human sensing [12, 52, 30]. RF-EATS’s goal is orthogonal to these proposals and it focuses on food and liquid sensing. It is worth noting that while some of these proposals can generalize to new multipath environments, their problem statement is fundamentally different than RF-EATS’s because the impact of the dielectric and multipath is not linearly separable as explained in §3.1.

(b) Use of Machine Learning in Wireless. Motivated by recent advances in machine learning, wireless researchers have adapted these advances to a variety of communication and sensing tasks, including end-to-end decoding [22], signal classification [48], localization [45, 68, 67, 69, 36], imaging [79], physiolog-

ical sensing [80], and spectrum monitoring [38, 20]. RF-EATS is similarly motivated by recent advances in learning; however, it focuses on the liquid sensing problem and introduces new contributions that allow it to address domain-specific challenges.

Finally, prior work on human activity sensing has recognized the problem of generalizing RF learning models to different environments [28, 80]. Existing solutions require collecting datasets for each activity and label across a large number of environments. In our context, this would require collecting measurements for each label/contaminant/class across a wide variety of environments, significantly increasing the training and data collection effort over RF-EATS’s approach. In contrast, RF-EATS’s multipath kernel and transfer learning approach allow it to generalize to new environments and sensing tasks in a sample-efficient manner.

6 Discussion & Conclusion

RF-EATS marks an important step toward ubiquitous, low-cost food sensing using pervasive networking technologies. Our evaluation demonstrated RF-EATS’s ability to deliver important applications, its resilience to changing indoor environments, and its efficiency in generalizing to new tasks and unseen environments.

RF-EATS’s design and evaluation can be extended in multiple ways. First, while our evaluation focused on changes in the radio environment (multipath reflections, positions, etc.), the RFID measurements may also be impacted by other environmental factors such as the shape and material of the container itself or even the impact of temperature changes on the dielectric. It may be possible to extend RF-EATS’s VAE to similarly learn the distributions of such changes and enable it to generalize to these environmental variables as well. We note that even without generalizing the model to different container shapes and materials, it can be used as-is in the context of counterfeit detection (e.g., fake perfume) since such items are typically designed to look very similar to the original products (but have different contents). Another valuable extension of RF-EATS is via miniaturization. Specifically, our current prototype is relatively bulky for direct consumer use. However, the large size is primarily due to the use of USRP software radios and log-periodic antennas for flexibility of prototyping, and can be miniaturized in future design iterations.

As the research evolves, we hope that it can continue bringing low-cost food and liquid sensing closer to the hands of lay consumers to help democratize food and product safety solutions.

Acknowledgments. We thank our shepherd Kyle Jamieson, the anonymous NSDI reviewers, and the Signal Kinetics group for their helpful feedback on the manuscript. This research is supported by a J-WAFS grant, the NSF, and the MIT Media Lab.

References

- [1] Alert for methanol. <https://foodsafety.neogen.com/en/alert-methanol>.
- [2] ALN-9640 Squiggle Inlay. www.alientechnology.com. Alien Technology Inc.
- [3] Children's tylenol cold & cough. <https://www.tylenol.ca/products/infants-children/childrens-tylenol-cold-cough>.
- [4] Counterfeit soft drinks? <https://www.ameribev.org/education-resources/blog/post/counterfeit-soft-drinks/>.
- [5] E8362B PNA Network Analyzer, 10 MHz to 20 GHz. <https://www.keysight.com/en/pd-72279-pn-E8362B/pna-series?cc=US&lc=eng>. keySight technologies.
- [6] Enfamil neuropro infant formula, ready to use. <https://www.enfamil.com/products/enfamil-neuropro-infant/8-fl-oz-ready-to-use-bottles-case-24>.
- [7] Extra virgin olive oil. <https://www.goya.com/en/products/extra-virgin-olive-oil>.
- [8] Graves grain alcohol 190@ - 750ml. <https://www.worldwidebev.com/graves-grain-alcohol-190at-4360.html>.
- [9] N1501A Dielectric Probe Kit. <https://www.keysight.com/en/pd-2492144-pn-N1501A/dielectric-probe-kit?cc=US&lc=eng>. keySight technologies.
- [10] Precision and recall. https://en.wikipedia.org/wiki/Precision_and_recall.
- [11] usrp n210. <http://www.ettus.com>, 2017. et-tus inc.
- [12] ADIB, F., HSU, C.-Y., MAO, H., KATABI, D., AND DURAND, F. Capturing the human figure through a wall. *ACM Transactions on Graphics (TOG)* 34, 6 (2015), 219.
- [13] AN, J., AND CHO, S. Variational autoencoder based anomaly detection using reconstruction probability.
- [14] AN, Z., LIN, Q., AND YANG, L. Cross-frequency communication: Near-field identification of uhf rfids with wifi! In *MobiCom* (2018), pp. 623–638.
- [15] ANG, P. K., CHEN, W., WEE, A. T. S., AND LOH, K. P. Solution-gated epitaxial graphene as ph sensor. *Journal of the American Chemical Society* 130, 44 (2008), 14392–14393.
- [16] BANERJEE, P., KINTZIOS, S., AND PRABHAKARPANDIAN, B. Biotoxin detection using cell-based sensors. *Toxins* 5, 12 (2013), 2366–2383.
- [17] BATTAN, C. How fake beauty products have infiltrated amazon, target, and other reliable retailers, 2017.
- [18] BHATTACHARYYA, R., FLOERKEMEIER, C., AND SARMA, S. Low-cost, ubiquitous rfid-tag-antenna-based sensing. *Proceedings of the IEEE* 98, 9 (2010), 1593–1600.
- [19] CUMMING, E. The great wine fraud, 2016.
- [20] DAVASLIOGLU, K., AND SAGDUYU, Y. E. Generative adversarial learning for spectrum sensing. In *2018 IEEE International Conference on Communications (ICC)* (2018), IEEE, pp. 1–6.
- [21] DHEKNE, A., GOWDA, M., ZHAO, Y., HAS-SANIEH, H., AND CHOUDHURY, R. R. Liquid: A wireless liquid identifier. In *ACM MobiSys* (2018).
- [22] FELIX, A., CAMMERER, S., DÖRNER, S., HOYDIS, J., AND TEN BRINK, S. Ofdm-autoencoder for end-to-end learning of communications systems. In *2018 IEEE 19th International Workshop on Signal Processing Advances in Wireless Communications (SPAWC)* (2018), IEEE, pp. 1–5.
- [23] FENG, C., LI, X., CHANG, L., XIONG, J., CHEN, X., FANG, D., LIU, B., CHEN, F., AND ZHANG, T. Material identification with commodity wi-fi devices. In *Proceedings of the 16th ACM Conference on Embedded Networked Sensor Systems* (2018), ACM, pp. 382–383.
- [24] GOSSNER, C. M.-E., SCHLUNDT, J., BEN EM-BAREK, P., HIRD, S., LO-FO-WONG, D., BELTRAN, J. J. O., TEOH, K. N., AND TRITSCHER, A. The melamine incident: implications for international food and feed safety. *Environmental health perspectives* 117, 12 (2009), 1803–1808.
- [25] HA, U., MA, Y., ZHONG, Z., HSU, T.-M., AND ADIB, F. Learning food quality and safety from wireless stickers. In *Proceedings of the 17th ACM Workshop on Hot Topics in Networks* (2018), ACM, pp. 106–112.

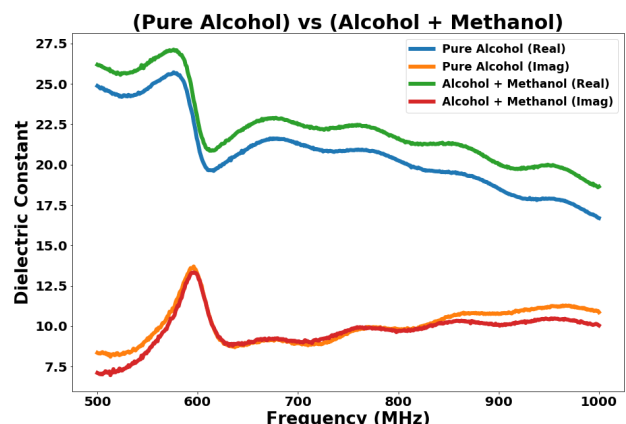
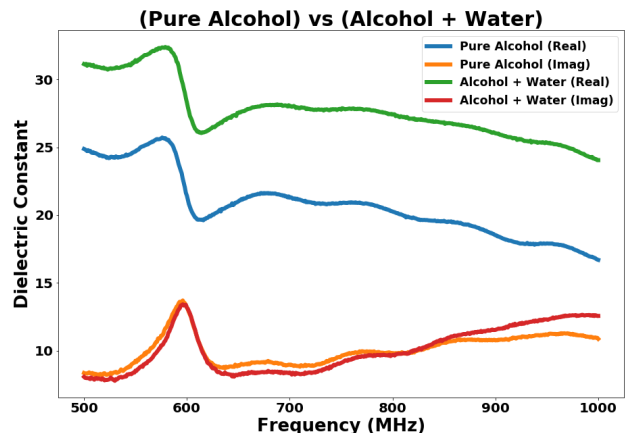
- [26] HENLEY, J. How to tell if your olive oil is the real thing, 2012.
- [27] HUANG, W.-D., CAO, H., DEB, S., CHIAO, M., AND CHIAO, J.-C. A flexible ph sensor based on the iridium oxide sensing film. *Sensors and Actuators A: Physical* 169, 1 (2011), 1–11.
- [28] JIANG, W., MIAO, C., MA, F., YAO, S., WANG, Y., YUAN, Y., XUE, H., SONG, C., MA, X., KOUTSONIKOLAS, D., ET AL. Towards environment independent device free human activity recognition. In *Proceedings of the 24th Annual International Conference on Mobile Computing and Networking* (2018), pp. 289–304.
- [29] JOHNSON, R. C., AND JASIK, H. Antenna engineering handbook. *New York, McGraw-Hill Book Company, 1984, 1356 p. No individual items are abstracted in this volume.* (1984).
- [30] JOSHI, K., BHARADIA, D., KOTARU, M., AND KATTI, S. Wideo: Fine-grained device-free motion tracing using {RF} backscatter. In *12th {USENIX} Symposium on Networked Systems Design and Implementation ({NSDI} 15)* (2015), pp. 189–204.
- [31] JOSHI, K., HONG, S., AND KATTI, S. Pinpoint: Localizing interfering radios. In *Usenix NSDI* (2013).
- [32] KARIMI, F. US warns travelers about tainted alcohol in Mexico. CNN, 2017. <http://www.cnn.com/2017/07/27/us/mexico-state-department-alcohol-warning/index.html>.
- [33] KINGMA, D. P., AND WELLING, M. Auto-encoding variational bayes. In *2nd International Conference on Learning Representations (ICLR)* (2013).
- [34] KOTARU, M., JOSHI, K., BHARADIA, D., AND KATTI, S. Spotfi: Decimeter level localization using wifi. In *ACM SIGCOMM computer communication review* (2015), vol. 45, ACM, pp. 269–282.
- [35] KUSWANDI, B., WICAKSONO, Y., ABDULLAH, A., HENG, L. Y., AHMAD, M., ET AL. Smart packaging: sensors for monitoring of food quality and safety. *Sensing and Instrumentation for Food Quality and Safety* 5, 3-4 (2011), 137–146.
- [36] LI, Q., QU, H., LIU, Z., ZHOU, N., SUN, W., AND LI, J. Af-dcgan: Amplitude feature deep convolutional gan for fingerprint construction in indoor localization system. *arXiv preprint arXiv:1804.05347* (2018).
- [37] LI, Z., AND SUSLICK, K. S. A hand-held optoelectronic nose for the identification of liquors. *ACS sensors* 3, 1 (2018), 121–127.
- [38] LI, Z., XIAO, Z., WANG, B., ZHAO, B. Y., AND ZHENG, H. Scaling deep learning models for spectrum anomaly detection. In *Proceedings of the Twentieth ACM International Symposium on Mobile Ad Hoc Networking and Computing* (2019), ACM, pp. 291–300.
- [39] LUO, Z., ZHANG, Q., MA, Y., SINGH, M., AND ADIB, F. 3d backscatter localization for fine-grained robotics. In *16th {USENIX} Symposium on Networked Systems Design and Implementation ({NSDI} 19)* (2019), pp. 765–782.
- [40] MA, Y., SELBY, N., AND ADIB, F. Minding the billions: Ultrawideband localization for deployed rfid tags. *ACM MobiCom* (2017).
- [41] MAKHZANI, A., SHLENS, J., JAITLEY, N., AND GOODFELLOW, I. Adversarial autoencoders. In *International Conference on Learning Representations* (2016).
- [42] NARSAIAH, K., JHA, S. N., BHARDWAJ, R., SHARMA, R., AND KUMAR, R. Optical biosensors for food quality and safety assurance: a review. *Journal of food science and technology* 49, 4 (2012), 383–406.
- [43] NEW YORK TIMES. China's Top Food Official Resigns. <http://www.nytimes.com/2008/09/23/world/asia/23milk.html>.
- [44] NGUYEN, D. S., LE, N. N., LAM, T. P., FRIBOURG-BLANC, E., DANG, M. C., AND TEDJINI, S. Development of novel wireless sensor for food quality detection. *Advances in Natural Sciences: Nanoscience and Nanotechnology* 6, 4 (2015), 045004.
- [45] NIITSOO, A., EDELHÄUSER, T., AND MUTSCHLER, C. Convolutional neural networks for position estimation in tdoa-based locating systems. In *2018 International Conference on Indoor Positioning and Indoor Navigation (IPIN)* (2018), IEEE, pp. 1–8.
- [46] ONG, K. G., BITLER, J. S., GRIMES, C. A., PUCKETT, L. G., AND BACHAS, L. G. Remote query resonant-circuit sensors for monitoring of bacteria growth: Application to food quality control. *Sensors* 2, 6 (2002), 219–232.

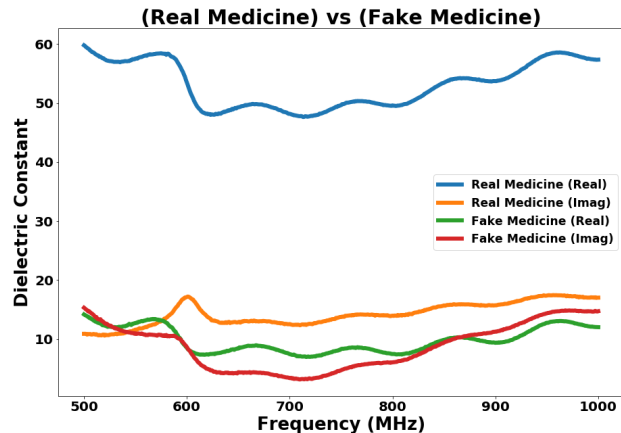
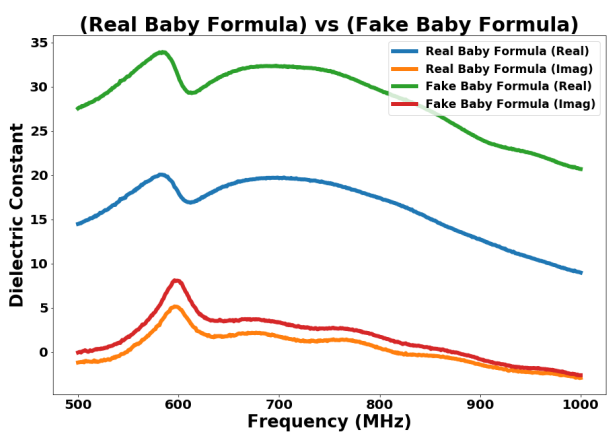
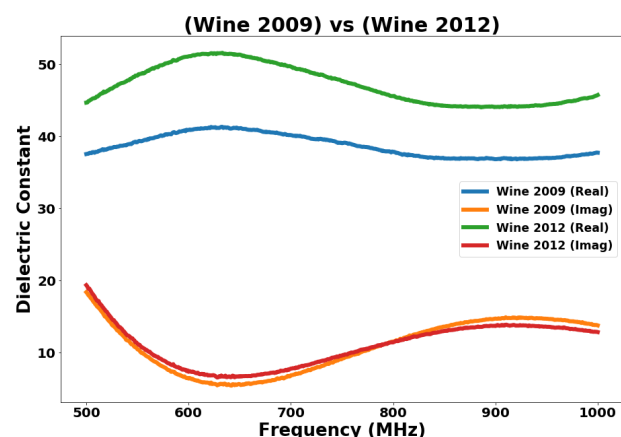
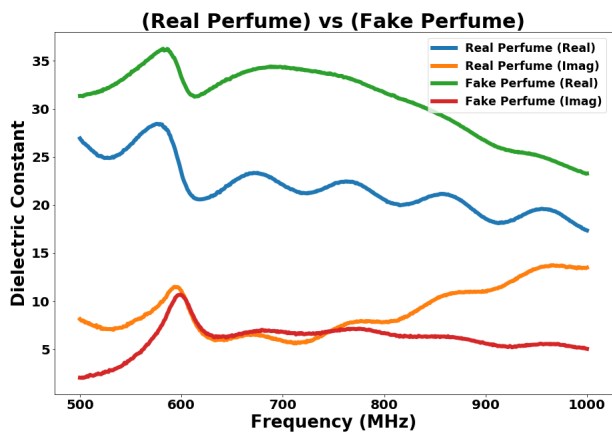
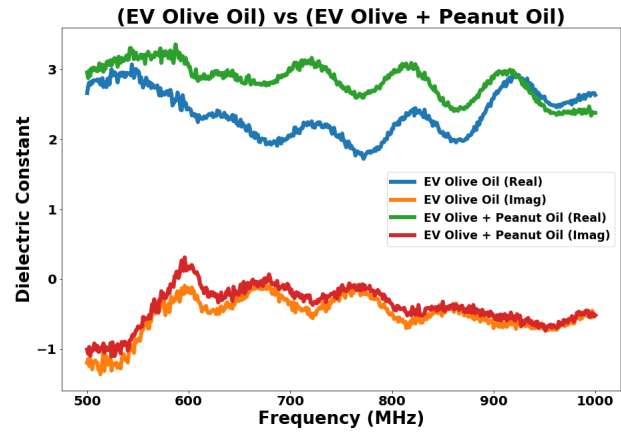
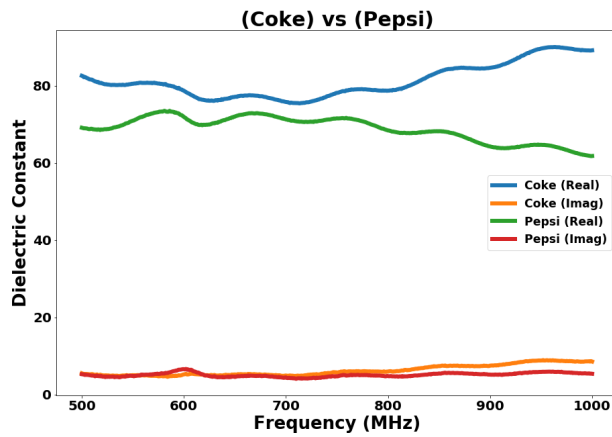
- [47] ONG, K. G., BITLER, J. S., GRIMES, C. A., PUCKETT, L. G., AND BACHAS, L. G. Remote query resonant-circuit sensors for monitoring of bacteria growth: Application to food quality control. *Sensors* 2, 6 (2002), 219–232.
- [48] O’SHEA, T. J., ROY, T., AND CLANCY, T. C. Over-the-air deep learning based radio signal classification. *IEEE Journal of Selected Topics in Signal Processing* 12, 1 (2018), 168–179.
- [49] PASZKE, A., GROSS, S., CHINTALA, S., CHANAN, G., YANG, E., DEVITO, Z., LIN, Z., DESMAISON, A., ANTIGA, L., AND LERER, A. Automatic differentiation in pytorch.
- [50] POLGREEN, L. 84 children are killed by medicine in nigeria, 2009.
- [51] POTYRAILO, R. A., NAGRAJ, N., TANG, Z., MONDELLO, F. J., SURMAN, C., AND MORRIS, W. Battery-free radio frequency identification (rfid) sensors for food quality and safety. *Journal of agricultural and food chemistry* 60, 35 (2012), 8535–8543.
- [52] PU, Q., JIANG, S., GOLLAKOTA, S., AND PATEL, S. Whole-home gesture recognition using wireless signals. In *ACM MobiCom* (2013).
- [53] PU, Y., GAN, Z., HENAO, R., YUAN, X., LI, C., STEVENS, A., AND CARIN, L. Variational autoencoder for deep learning of images, labels and captions. In *Advances in neural information processing systems* (2016), pp. 2352–2360.
- [54] PUREFOY, C. Poisoned medicine kills dozens of children in nigeria, 2008.
- [55] RADFORD, A., METZ, L., AND CHINTALA, S. Unsupervised representation learning with deep convolutional generative adversarial networks. *arXiv preprint arXiv:1511.06434* (2015).
- [56] RAHMAN, T., ADAMS, A. T., SCHEIN, P., JAIN, A., ERICKSON, D., AND CHOUDHURY, T. Nutrilyzer: A mobile system for characterizing liquid food with photoacoustic effect. In *Proceedings of the 14th ACM Conference on Embedded Network Sensor Systems CD-ROM* (2016), ACM, pp. 123–136.
- [57] RAHMAN, T., ADAMS, A. T., SCHEIN, P., JAIN, A., ERICKSON, D., AND CHOUDHURY, T. Nutrilyzer: A mobile system for characterizing liquid food with photoacoustic effect. In *Proceedings of the 14th ACM Conference on Embedded Network Sensor Systems CD-ROM* (New York, NY, USA, 2016), SenSys ’16, ACM, pp. 123–136.
- [58] RUCH, P., HU, R., CAPUA, L., TEMIZ, Y., PAREDES, S., LOPEZ, A., BARROSO, J., COX, A., NAKAMURA, E., AND MATSUMOTO, K. A portable potentiometric electronic tongue leveraging smartphone and cloud platforms. pp. 1–3.
- [59] SMARTRAC GROUP. Smartrac Shortdipole Inlay. www.smartrac-group.com.
- [60] SRIDHAR, M., AND REDDY, C. R. Surface tension of polluted waters and treated wastewater. *Environmental Pollution Series B, Chemical and Physical* 7, 1 (1984), 49–69.
- [61] SUN, C., AND TRUEMAN, C. W. Unconditionally stable crank-nicolson scheme for solving two-dimensional maxwell’s equations. *Electronics Letters* 39, 7 (April 2003), 595–597.
- [62] TAN, E. L., NG, W. N., SHAO, R., PERELES, B. D., AND ONG, K. G. A wireless, passive sensor for quantifying packaged food quality. *Sensors* 7, 9 (2007), 1747–1756.
- [63] TSE, D., AND VISWANATH, P. *Fundamentals of wireless communication*. Cambridge university press, 2005.
- [64] ULABY, F. T., MICHELSSEN, E., AND RAVAIOLI, U. Fundamentals of applied electromagnetics 6e. Boston, Massachusetts: Prentice Hall (2010).
- [65] VASILESCU, A., AND MARTY, J.-L. Electrochemical aptasensors for the assessment of food quality and safety. *TrAC* 79 (2016), 60–70.
- [66] WANG, J., XIONG, J., CHEN, X., JIANG, H., BALAN, R., AND FANG, D. Tagscan: Simultaneous target imaging and material identification with commodity rfid devices. *ACM MobiCom* (2017).
- [67] WANG, X., GAO, L., AND MAO, S. Csi phase fingerprinting for indoor localization with a deep learning approach. *IEEE Internet of Things Journal* 3, 6 (2016), 1113–1123.
- [68] WANG, X., GAO, L., MAO, S., AND PANDEY, S. Csi-based fingerprinting for indoor localization: A deep learning approach. *IEEE Transactions on Vehicular Technology* 66, 1 (2016), 763–776.
- [69] WANG, X., WANG, X., AND MAO, S. Cifi: Deep convolutional neural networks for indoor localization with 5 ghz wi-fi. In *2017 IEEE International Conference on Communications (ICC)* (2017), IEEE, pp. 1–6.

- [70] WANG, Y. In Flint, Mich., there's so much lead in children's blood that a stat of emergency is declared. *The Washington Post*, 2015. <https://www.washingtonpost.com/news/morning-mix/wp/2015/12/15/toxic-water-soaring-lead-levels-in-childrens-blood-create-state-of-emergency-in-flint-mich/>.
- [71] WEI, M., HUANG, S., WANG, J., LI, H., YANG, H., AND WANG, S. The study of liquid surface waves with a smartphone camera and an image recognition algorithm. *European Journal of Physics* 36, 6 (2015), 065026.
- [72] WU, S.-Y., YANG, C., HSU, W., AND LIN, L. 3d-printed microelectronics for integrated circuitry and passive wireless sensors. *Microsystems & Nanoengineering* 1 (2015), 15013.
- [73] XIONG, J., AND JAMIESON, K. ArrayTrack: a fine-grained indoor location system. In *Usenix NSDI* (2013).
- [74] YANZI, Z., YIBO, Z., BEN, Y. Z., AND HAITAO, Z. Reusing 60ghz radios for mobile radar imaging. In *ACM MobiCom* (2015).
- [75] YEO, H.-S., FLAMICH, G., SCHREMPF, P., HARRIS-BIRTILL, D., AND QUIGLEY, A. Radarcat: Radar categorization for input & interaction. In *Proceedings of the 29th Annual Symposium on User Interface Software and Technology* (2016), ACM, pp. 833–841.
- [76] YOON, J.-Y., AND KIM, B. Lab-on-a-chip pathogen sensors for food safety. *Sensors* 12, 8 (2012), 10713–10741.
- [77] YUE, S., AND KATABI, D. Liquid testing with your smartphone. In *Proceedings of the 17th Annual International Conference on Mobile Systems, Applications, and Services* (2019), ACM, pp. 275–286.
- [78] ZHANG, J., AND TIAN, G. Y. Uhf rfid tag antenna-based sensing for corrosion detection & characterization using principal component analysis. *IEEE TAP* 64, 10 (2016), 4405–4414.
- [79] ZHAO, M., TIAN, Y., ZHAO, H., ALSHEIKH, M. A., LI, T., HRISTOV, R., KABELAC, Z., KATABI, D., AND TORRALBA, A. Rf-based 3d skeletons. In *Proceedings of the 2018 Conference of the ACM Special Interest Group on Data Communication* (2018), ACM, pp. 267–281.
- [80] ZHAO, M., YUE, S., KATABI, D., JAAKKOLA, T. S., AND BIANCHI, M. T. Learning sleep stages from radio signals: a conditional adversarial architecture. In *International Conference on Machine Learning* (2017), pp. 4100–4109.

A Dielectric Measurements

To ensure there is a detectable difference between the real and contaminated/fake products, we measured the dielectric constants of each of the materials. We used the Keysight N1501A Dielectric Probe Kit and E8362B PNA Network Analyzer. We calibrated the dielectric probe with 20°C water and performed a linear sweep from 500MHz to 1GHz, in steps of 1 MHz. The graphs below plot the dielectric constants as a function of frequency.





B Results of Multiclass Classification

Fig. 13 plots the confusion matrix table for multiclass classification between all the tested contents. Training and testing regime performed in different environments similar to Fig. 7(b). The different rows of the matrix represent the actual class of the samples, while the different columns represent RF-EATS's predicted class. The overall accuracy is 85.8%.

A	Alcohol			B	Alcohol+Water		
C	Alcohol+Methanol			D	Coke		
E	Diet Coke			F	Pepsi		
G	Olive Oil			H	Olive Oil + Peanut Oil		
I	Baby Formula			J	Adulterated Baby Formula		
K	Perfume			L	Fake Perfume		
M	Medicine			N	Fake Medicine		
O	Wine (2009)			P	Wine (2012)		

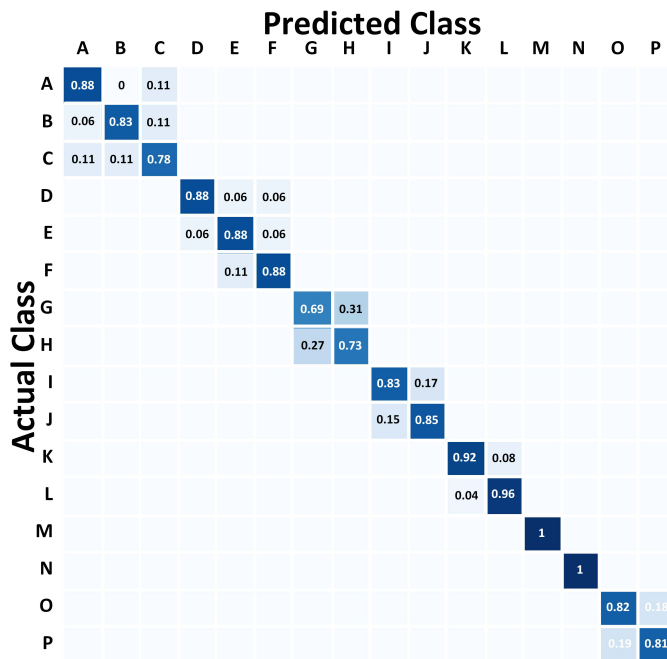


Figure 13: Confusion Matrix